nature geoscience

Article

https://doi.org/10.1038/s41561-024-01608-w

Increased urban ozone in heatwaves due to temperature-induced emissions of anthropogenic volatile organic compounds

Received: 11 June 2024

Accepted: 30 October 2024

Published online: 2 January 2025

Check for updates

Momei Qin[1], Yongliang She[1], Ming Wang[1], Hongli Wang[2], Yunhua Chang[3], Zhaofeng Tan[4], Jingyu An[2,5], Jian Huang[6], Zibing Yuan[7], Jun Lu[2], Qian Wang[2], Cong Liu[8], Zhenxin Liu[1], Xiaodong Xie[1], Jingyi Li[1], Hong Liao[1], Havala O. T. Pye[9], Cheng Huang[10], Song Guo[4], Min Hu[4], Yuanhang Zhang[4], Daniel J. Jacob[11] & Jianlin Hu[1]

Urban ozone (O_3) pollution correlates with temperature, and higher O_3 often occurs during heatwaves, threatening public health. However, limited data on how anthropogenic volatile organic compound (AVOC) precursor emissions vary with temperature hinders understanding their impact on O_3. Here we show that the increase in non-combustion AVOC emissions (for example, from volatile chemical products) during a heatwave in Shanghai contributes significantly to increased O_3, on the basis of ambient measurements, emissions testing and air quality modelling. AVOC concentrations increase ~twofold when the temperature increases from 25 °C to 35 °C due to air stagnation and increased emissions. During the heatwave, higher concentrations result in an 82% increase in VOC OH reactivity. Air quality simulations reveal that temperature-driven AVOC emissions increases account for 8% (1.6 s^{-1}) of this reactivity increase and enhance O_3 by 4.6 ppb. Moreover, we predict a more profound (twofold) increase in OH reactivity of oxygenated VOCs, facilitating radical production and O_3 formation. Enhanced AVOC emissions trigger O_3 enhancements in large cities in East China during a heatwave, and similar effects may also happen in other AVOC-sensitive megacities globally. Reducing AVOC emissions, particularly non-combustion sources, which are currently less understood and regulated, could mitigate potential O_3 pollution in urban environments during heatwaves.

Surface ozone (O_3) is a harmful air pollutant that affects public health and ecosystems[1,2]. This pollutant is produced by photochemical reactions involving volatile organic compounds (VOCs) and nitrogen oxides ($NO_x \equiv NO + NO_2$) (ref. 3). NO_x originates mainly from fuel combustion, while most VOCs are emitted from combustion, solvent evaporation during the manufacturing and use of volatile chemical products (VCPs, also known as solvent use), industrial activities and vegetation[4,5]. Moreover, anthropogenic VOCs (AVOCs) are substantial contributors to O_3 formation in urban areas worldwide[6–8].

Ozone air pollution is strongly correlated with temperature, amplifying the public health risks associated with heatwaves (persistent temperature extremes)[9,10]. This O_3–temperature correlation has been explained by meteorological covariates (clear skies and stagnation) and enhanced VOC emissions from vegetation[11–13]. However, an additional factor could be the elevated AVOC emissions,

A full list of affiliations appears at the end of the paper. e-mail: jianlinhu@nuist.edu.cn

https://doi.org/10.1038/s41561-024-01608-w

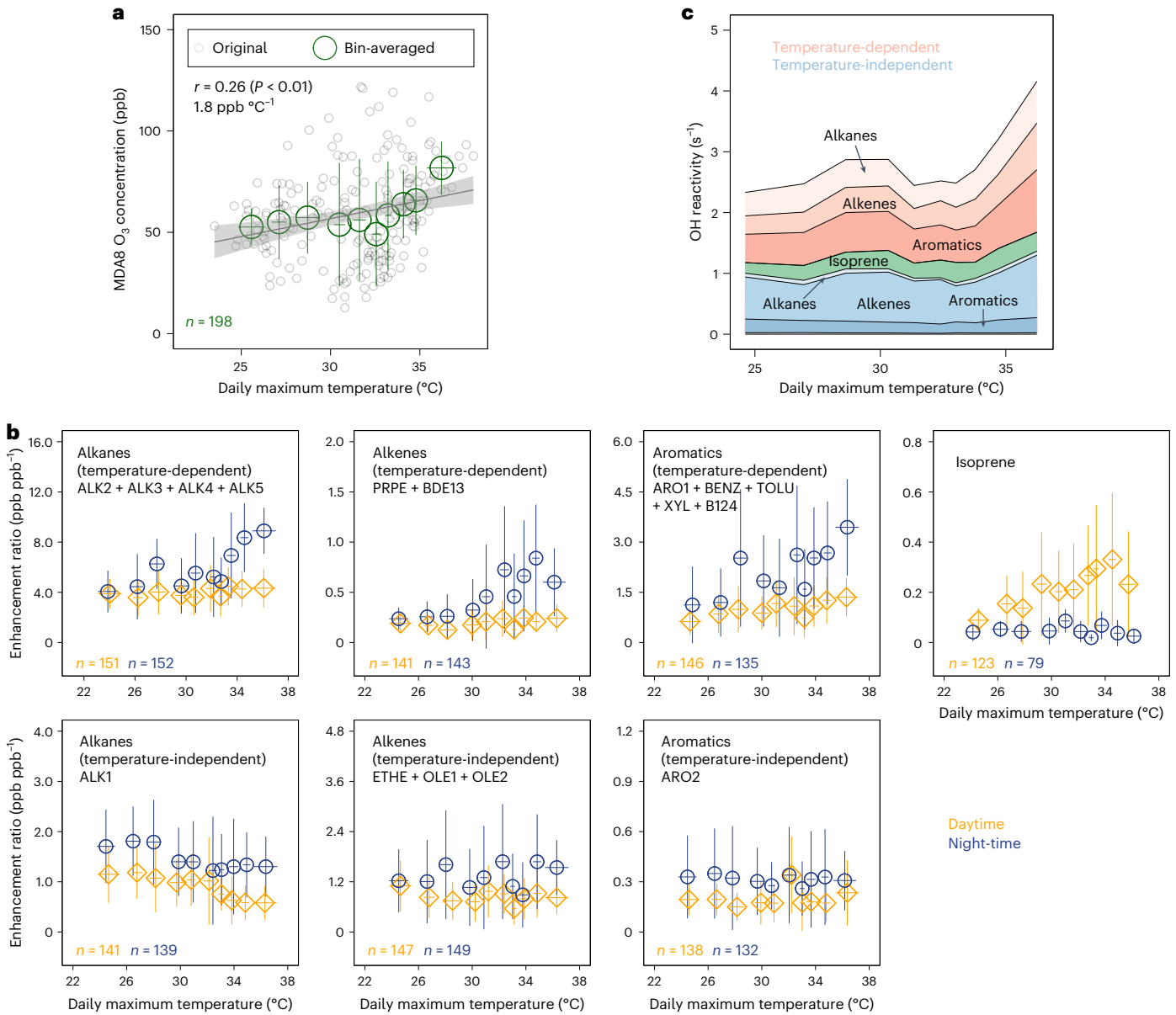

Fig. 1 | O_3 concentration, VOC ERs and OH reactivity versus temperature during the summers of 2018–2020 in Shanghai. a, Observed MDA8 O_3 level versus temperature at the sites supervised by the China National Environmental Monitoring Centre (CNEMC) in Shanghai. **b**, Observed daytime (10:00–18:00 LT) and night-time (22:00–06:00 LT) ERs of VOC groups versus temperature, with the top (bottom) row showing temperature-dependent (temperature-independent) VOCs, based on the measurements on weekdays at the Shanghai Academy of Environmental Sciences (SAES) site. In **a** and **b**, daily O_3 and ERs (with the sample size shown in the lower left corner of each panel) were split evenly into ten bins according to the paired temperatures. The average values for O_3, daytime ER and night-time ER in each bin are represented by green (in **a**), yellow and blue (in **b**) open circles, respectively, with the standard deviations (±1σ) represented by whiskers. The grey circles in **a** represent daily O_3 levels, with a linear least-squares regression line and light grey shading indicating the 95% confidence interval. The definitions of individual VOCs using the SAPRC07tic chemical mechanism in **b** are shown in Supplementary Table 3. **c**, OH reactivity contributed by temperature-dependent VOCs (red) and temperature-independent VOCs (blue) according to the measured VOCs in **b**. ALK1–5, alkanes; ARO1 and ARO2, aromatics that are not explicitly represented; BDE13, 1,3-butadiene; BENZ, benzene; B124, 1,2,4-trimethylbenzene; ETHE, ethene; OLE1 and OLE2, alkenes that are not explicitly represented; PRPE, propene; TOLU, toluene; XYL, xylenes.

particularly from non-combustion sources such as VCPs. Recent flux measurements in Los Angeles provided direct and compelling evidence that emissions of AVOC markers, including toluene, ethanol and para-chlorobenzotrifluoride, increase with temperature, following vapour pressure curves[14]. The temperature dependency of AVOC concentrations has also been observed in New York City and the Los Angeles Basin[15,16]. Moreover, in the San Joaquin Valley of California, total VOC OH reactivity (hereafter referred to as OH reactivity) was dominated by temperature-dependent VOCs at high temperatures[17]. Early experiments indicated that temperature affects vehicular non-tailpipe emissions[18–20]. In addition, emissions of formaldehyde (HCHO) or other VOCs from building and automobile materials are strongly dependent on temperature[21–24]. A box modelling study further revealed that temperature-dependent AVOC emissions could increase O_3 levels by several parts per billion in urban environments[12].

Heatwaves are projected to increase as the climate changes, causing more episodes of elevated O_3 levels[25]. The increasing prevalence of these events could become the top risk for the global health burden[9,10].

https://doi.org/10.1038/s41561-024-01608-w

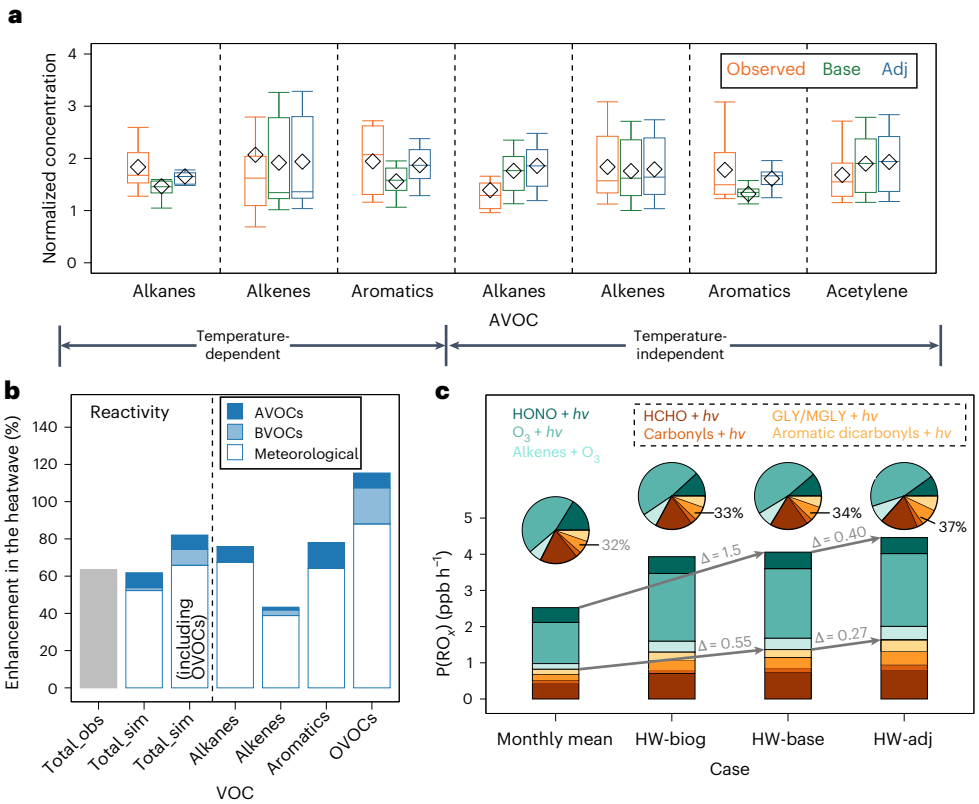

Fig. 2 | Enhancements in VOC concentrations, OH reactivity and radical production at high temperatures. a, AVOC concentrations at temperatures greater than 35 °C (over 9 days) normalized to the average concentrations in the temperature range of 20–30 °C at the SAES site during the summer of 2018. The horizontal lines and squares represent medians and mean values, respectively, with the edges of boxes representing the 25th and 75th percentiles. The whiskers indicate the minimum and maximum values. **b**, Simulated enhancements of OH reactivity during the heatwave (25–30 July) relative to the monthly averages. The enhancement of total OH reactivity based on the VOC measurements (not including OVOCs) is shown in grey compared with simulations with or without OVOCs in the adj case. The impacts induced by meteorological conditions, BVOCs and AVOCs are indicated with transparent, semi-transparent and solid bars, respectively. **c**, Simulated $P(RO_x)$ (bars) and relative contributions of major reactions (pies) in different cases (Methods). The cases labelled 'HW' indicate average values during the heatwave. In the pie chart, the black numbers indicate the relative contributions of photolysis of carbonyl compounds. Changes in total and carbonyl-related $P(RO_x)$ between different cases are indicated by the grey numbers. All carbonyl-related reactions are outlined with dashed lines in the legend. GLY, glyoxal; MGLY, methylglyoxal.

Recent research has highlighted that temperature-dependent terpenoid emissions from vegetation dominate O_3 formation at high temperatures in Los Angeles[14]. However, no previous studies have considered the role of increased AVOC emissions in response to high temperatures, which limits the knowledge of the O_3 climate penalty and associated health risks in urban areas.

Here we probe the linkage between the observed AVOC levels and temperature in Shanghai, a megacity located in the Yangtze River Delta (YRD) in East China with strong emissions of AVOCs, including substantial solvent use[26–28], potentially modulated by temperature. We incorporate experimentally derived AVOC emissions variations with temperature into the Community Multiscale Air Quality (CMAQ) model and infer the role of increased AVOC emissions in contributing to elevated O_3 levels during heatwaves.

Observed dependence of AVOC emissions on temperature

The observations in Shanghai indicate increasing O_3 and VOC concentrations with increasing temperatures in summer. The maximum daily average 8 hour (MDA8) O_3 concentration over three summers (2018–2020) was positively correlated with temperature and increased at 1.8 ppb $°C^{-1}$ (Fig. 1a). The NO_2 concentration did not correlate with temperature (Supplementary Fig. 1), but the levels of 34 individual AVOCs were positively correlated with temperature ($P < 0.01$; Supplementary Table 1), hereafter referred to as temperature-dependent AVOCs. Figure 1b shows the variation in measured VOCs (all hydrocarbons) grouped by functional type and temperature dependence, expressed as an enhancement ratio (ER (Methods); ERs for individual VOCs are shown in Extended Data Fig. 1) relative to acetylene, a long-lived tracer of fossil fuel combustion uncorrelated with temperature and used to correct for the effect of dilution (for example, enhanced convective mixing under warm conditions or, conversely, air stagnation when heat extremes occur[12,29]). Among these VOCs, the ERs of most alkanes, propene, 1,3-butadiene, benzene, toluene, xylenes and other less-reactive aromatics generally increased with temperature, particularly at night (when photochemistry ceased) and at high temperatures, with moderate positive correlations with daily maximum temperature ($r \geq 0.3$ with $P < 0.01$; Supplementary Table 2).

The variation in VOCs with temperature propagated to changes in OH reactivity. The identified temperature-dependent AVOCs contributed substantially to the total OH reactivity (50–60%; Fig. 1c) and exhibited a twofold increase in reactivity at high temperatures (>35 °C versus 25 °C). As a result, the total OH reactivity increased under warmer conditions. Moreover, the coincident temperature dependence observed in O_3 and OH reactivity implies a possible correlation between the two variables in Shanghai, highlighting the importance of elucidating the drivers behind increases in AVOCs at higher temperatures. The increase in ERs (without dilution effects) with increasing temperature, along with the absence of secondary sources for the measured hydrocarbons,

https://doi.org/10.1038/s41561-024-01608-w

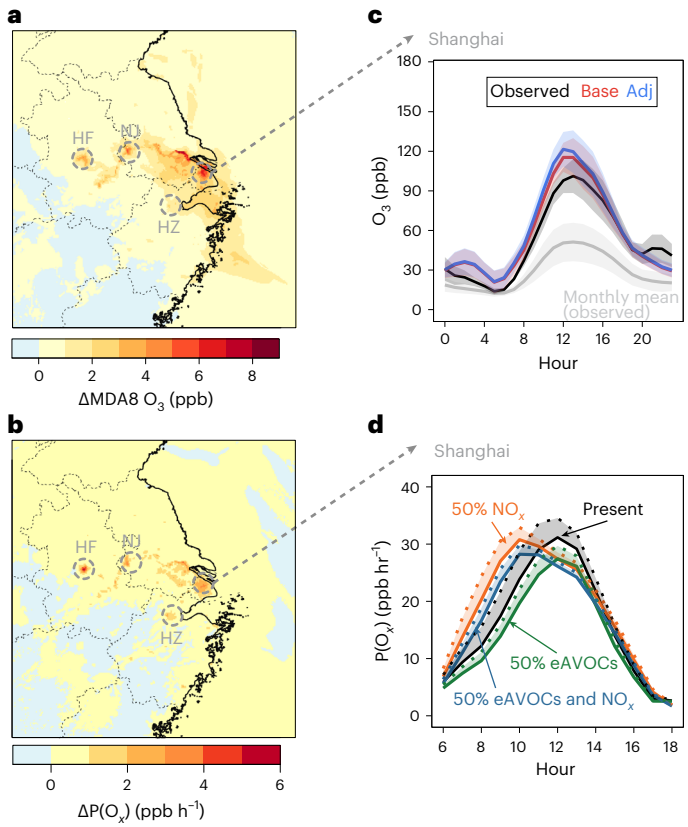

Fig. 3 | Impacts of AVOC emissions enhancements on O_3 chemistry during the heatwave. a,**b**, Simulated changes in MDA8 O_3 (**a**) and the daytime (6:00–18:00 LT) $P(O_x)$ (**b**) in the YRD. Large cities are marked with circles. **c**,**d**, Diurnal variations in O_3 (**c**) and $P(O_x)$ (**d**) in Shanghai. The shaded areas in **c** represent ±0.5σ from the averages. The shaded areas in **d** indicate the differences between the cases with (dotted lines) and without (solid lines) the temperature effect of AVOC emissions. Changes in $P(O_x)$ were examined under four emissions scenarios: (1) present emissions (black), (2) a 50% reduction in NO_x (orange), (3) a 50% reduction in evaporative emissions of AVOCs (eAVOCs; green) and (4) concurrent reductions in both NO_x and eAVOCs (blue).

collectively indicates an important role for increasing VOC emissions when temperatures are higher.

The individual VOC species driving the temperature dependence of total OH reactivity were further examined to identify the sources of emissions. Vehicle tailpipe emissions are unlikely to drive the overall increase in VOC with temperature since acetylene and NO_2 (both of which are traffic tracers in urban areas) did not significantly increase at higher temperatures (Supplementary Figs. 1 and 2), and previous work for vehicles indicates that tailpipe emissions are temperature-independent[15,17]. The top five temperature-dependent VOCs that contributed appreciably to OH reactivity included m/p-xylene, propene, t-2-butene, toluene and o-xylene (Supplementary Table 4). These VOCs are indicative of non-combustion (or evaporative) emissions, including VCPs (for example, paint, printing and asphalt) and other vapour pressure-driven emissions (for example, gasoline evaporation and storage tank evaporation)[30–34], consistent with solvent use being a prominent VOC source in Shanghai and surrounding areas inferred from top-down[27,34] and bottom-up estimates (Supplementary Figs. 3 and 4). In addition, some species possibly associated with the petrochemical industry (for example, propene and 1,3-butadiene) exhibited temperature sensitivity, and the temperature dependence of this source has been previously reported[17,35].

Attribution of VOC enhancements during a heatwave

To further isolate AVOC emissions changes during a major heatwave on 25–30 July 2018, we conducted two CMAQ simulations for summer 2018: one with (adjusted (adj)) and one without (base case) day-to-day variations in AVOC emissions from non-combustion sources related to temperature (Methods). An additional simulation for the heatwave event was performed using monthly average biogenic emissions (HW_biog case) to elucidate the impact of temperature-induced changes in biogenic emissions compared with the base case. The source-specific AVOC emissions changes in the adj case better reflected the observed increase in temperature-dependent alkanes and aromatics by ~twofold at >35 °C versus 25 ± 5 °C and resulted in higher measurement–simulation correlations than those in the base simulation (Fig. 2a and Supplementary Table 5). As the temperature effects on some industrial emissions were missing in the model, temperature-dependent alkenes were unchanged. The increase in temperature-dependent alkanes remained biased low, also indicating that the adj case may underestimate the role of temperature in increasing AVOC emissions.

The total OH reactivity inferred in Shanghai from all measured VOCs was enhanced by 63% during the heatwave, substantially higher than the predicted increase in emissions (Fig. 2b and Extended Data Fig. 2). The reactivity increase was captured well by the model, which indicates a total reactivity enhancement of 82% when oxygenated VOCs (OVOCs, not measured) were accounted for. Such notable changes in OH reactivity (resulting from increased VOC concentrations) were facilitated primarily by meteorological processes, including reductions in wind speed, and thus suppressed horizontal transport of VOCs (Supplementary Figs. 5 and 6). AVOC emissions accounted for approximately 8% (1.6 s^{-1}) of the overall increase of 82% in OH reactivity, comparable to the increase of 9% induced by biogenic emissions changes (Methods and Supplementary Table 6). Among all the VOC groups, the reactivity of aromatics was the most susceptible to temperature-dependent AVOC emissions fluctuations.

The predicted OH reactivity of OVOCs was more than twice as high as the monthly average reactivity during the heatwave. The major contributors included aldehydes, ketones, ethanol and aromatic-derived dicarbonyl compounds (Supplementary Fig. 7). This finding was consistent with the measurement in San Joaquin Valley, which showed that the reactivity of small aldehydes and alcohols increased substantially at high temperatures[17]. We also observed a strong temperature dependency of aldehyde and ketone levels in Hangzhou (Extended Data Fig. 3). Given that the relative enhancement of OVOC reactivity surpassed that of all hydrocarbon systems and that HCHO had relatively few primary sources in the model (Supplementary Fig. 8), the temperature effect on OVOCs was driven by the efficient production of secondary OVOCs rather than increases in OVOC emissions during the heatwave. Therefore, we inferred that both the accumulation of VOC precursors and high atmospheric oxidizing capacity (as indicated by OH radical levels; Supplementary Fig. 9) promoted the chemical formation of OVOCs with heat extremes. Specifically, AVOC emissions were responsible for 8% of the overall increase in OVOC reactivity (up to 15.4% for major OVOCs; Supplementary Fig. 10) versus 19% for biogenic VOC (BVOC) emissions.

The modelled emissions of primary OVOCs also exhibited strong sensitivity to temperature (Supplementary Fig. 11). However, OVOC emissions, such as those of alcohols, glycols, ketones, glycol ethers and esters, may have been underestimated or misrepresented in the models due to the uncertainties associated with VCP emissions estimates and condensed chemical mechanisms[4,36–38]. The flux measurements in Los Angeles confirmed the temperature dependency of OVOC emissions[14]. Despite contributing ~60% of the VOC mass flux at high temperatures, OVOCs accounted for only ~20% of the OH reactivity, probably due to their relatively low reactivity. The contribution of OVOCs to the OH reactivity of emissions varies across different VCP sources, ranging from 15% in ship coating to over 70% in printing and other

https://doi.org/10.1038/s41561-024-01608-w

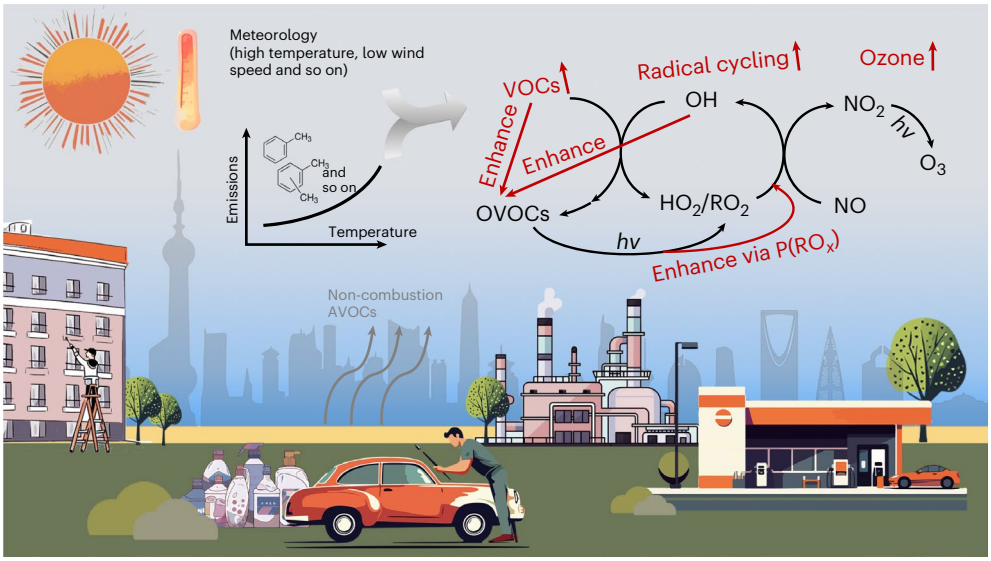

Fig. 4 | How temperature-induced AVOC emissions are likely to exaggerate O_3 pollution in AVOC-sensitive megacities during heatwaves. Increased AVOC emissions from anthropogenic non-combustion sources enhance OVOC concentrations, promoting radical production and O_3 formation during heatwaves.

industrial coatings[39]. The impact of increases in these OVOC emissions on photochemistry at high temperatures warrants further evaluation.

The increases in OVOCs during heatwaves represented chemical feedback in response to the climatic event. Among OVOCs, carbonyls (in particular, HCHO) have been regarded as photochemical amplifiers because they provide primary sources of RO_x radicals ($RO_x = OH + HO_2 + RO_2$) to drive O_3 production[40–42]. According to the CMAQ simulation, the photolysis of HCHO and other carbonyl compounds was responsible for ~32% of the daytime primary radical source ($P(RO_x)$) in July and ~37% during the heatwave in Shanghai (Methods, Fig. 2c and Supplementary Table 7), which is consistent with other Chinese megacities[43,44]. In the base case, the total $P(RO_x)$ during the heatwave was 1.5 ppb h^{-1} (~60%) higher than the monthly mean. The AVOC emissions changes further increased the $P(RO_x)$ by 0.40 ppb h^{-1}, which was attributed predominantly to the photolysis of HCHO and dicarbonyl compounds (0.27 ppb h^{-1}), with the remaining increases induced by higher O_3 concentrations. Thus, temperature-dependent AVOC emissions ultimately exacerbate O_3 pollution by producing more carbonyls with higher $P(RO_x)$ during heatwaves in urban environments. However, the overall effect of biogenic emissions enhancement on the $P(RO_x)$ increase was lower than the AVOC-induced impact in Shanghai. It is worth noting that isoprene dominated HCHO sources in New York City[45], indicating potentially different roles of AVOC and BVOC emissions in $P(RO_x)$ increases across megacities, depending on local emissions profiles.

Effects on the O_3 concentration during heatwaves

With warming-induced emissions changes, increased VOC concentrations leading to increased OH reactivity and RO_x production facilitated O_3 formation at high temperatures. In urban Shanghai, the O_3 concentration was persistently high during the heatwave (Extended Data Fig. 4). The modelled (observed) MDA8 O_3 concentration was ~46 ppb (42 ppb) higher than the monthly mean in July 2018, which was attributable primarily to meteorological conditions (Supplementary Table 8). The changes in the BVOC and AVOC emissions had almost equal impacts on the increase in O_3. Specifically, the AVOC emissions enhancements led to an increase of 4.6 ppb for MDA8 O_3 and an increase of 7.5 ppb in peak O_3, equivalent to a 5–7% enhancement on top of the base case in Shanghai (Fig. 3c). It is important to note that only approximately half of the daytime O_3 was associated with local emissions in the YRD (Methods and Extended Data Fig. 5), and the O_3 that is predominantly impacted by the region-wide evaporative AVOC emissions increased by 45% due to the temperature effect.

The daytime O_x net production ($P(O_x)$, $O_x = O_3 + NO_2$) in the CMAQ simulation was also greater than the monthly average during the heatwave in the base case (15.9 ppb hr^{-1} versus 10.7 ppb hr^{-1}). The AVOC emissions changes at higher temperatures gave rise to an additional increase of 2.5 ppb hr^{-1} in $P(O_x)$ (Fig. 3d) and explained 5% of the total enhancement of 54% during the heatwave relative to the monthly average. The increases in MDA8 O_3 and daytime $P(O_x)$ (ΔMDA8 O_3 and $\Delta P(O_x)$ in Fig. 3a,b) levels were predicted to be distinct in other large cities in East China, for example, Hangzhou, Nanjing and Hefei. Notably, we observed the concurrent temperature dependence of AVOC and O_3 levels in Hangzhou (Extended Data Fig. 3 and Supplementary Fig. 12). The association between elevated O_3 levels and increased AVOC emissions could exist in other city centres where O_3 is sensitive to AVOCs.

The impacts of reductions in anthropogenic emissions on O_3 chemistry during the heatwave were assessed under several emissions scenarios (Methods). Figure 3d shows that a 50% reduction in evaporative AVOC emissions led to a decrease in the maximum $P(O_x)$ of 14% in Shanghai during the event, which was more significant than the 50% reduction in NO_x (5%) and nearly as effective as both reductions applied. A more substantial decrease (36%) in $P(O_x)$ could be achieved with a 50% reduction in AVOC emissions from all sources (Supplementary Fig. 13). These results indicate that AVOC emissions control has the potential to mitigate urban O_3 during heatwaves. The estimated $\Delta P(O_x)$ induced by AVOC enhancements during the heatwave ranged from 1.0 to 1.7 ppb hr^{-1} with emissions reductions, lower than 2.5 ppb hr^{-1} for the current emissions (Supplementary Table 9). Therefore, reducing anthropogenic emissions, whether VOCs or NO_x, would diminish the impact of temperature-driven AVOC emissions changes on photochemistry.

While we emphasize AVOC emissions reductions in megacities, it should not be assumed that NO_x reductions are insignificant. Although O_3 levels were suppressed by NO_x emissions in the morning, there was a transition to a positive O_3 response at noon in Shanghai during the heatwave (Supplementary Fig. 14). This suggests that NO_x reductions are effective in lowering elevated urban O_3 in the afternoon, especially as evaporative AVOC emissions increase with temperature. In addition, NO_x reductions were beneficial to O_3 abatement on a regional

scale (Supplementary Fig. 15) and weakened the sensitivity of O_3 to increases in evaporative AVOC emissions (or similarly biogenic emissions in forested areas) during heatwaves (Supplementary Figs. 16–17). In recent decades, some areas in the US and China have shifted from a predominantly VOC-limited regime to a transitional or NO_x-limited regime, driven by a rapid decline in NO_x emissions[6,7]. With projected continued NO_x reductions, O_3 might become more sensitive to NO_x. Therefore, tighter NO_x emissions controls should be considered in future regional, long-term strategies for O_3 mitigation.

Implications for ozone pollution control during heatwaves

AVOC emissions in Shanghai in summer increase during a heatwave, mainly from non-combustion sources (largely VCP-related sources). In addition to meteorological conditions conducive to photochemistry (for example, clear skies), higher AVOC emissions and air stagnation lead to the accumulation of VOCs, triggering elevated O_3 levels. OVOCs, which are readily formed with high oxidants at high temperatures, amplify the effect of abundant VOC precursors by providing radical primary sources (Fig. 4). As we show that increases in AVOC emissions increase O_3 levels in large cities in East China, the impact could be noticeable across other megacities that experience VOC-limited/transition O_3 regimes globally.

To date, non-combustion sources, which are potentially temperature-dependent, account for approximately half of the AVOC emissions in China and the US[4,5,46]. Given the expected stringent controls on combustion sources (particularly for synergistic reductions in CO_2 emissions with carbon neutrality policies), future AVOC emissions might become increasingly sensitive to temperature[4,15,17,20,47,48]. Recent measurements of aromatics in the Los Angeles Basin from 2010 to 2018 showed a greater correlation with temperature than did the observations in earlier years (1999–2009)[16]. Because of the strong temperature dependence of hazardous air pollutants, such as toluene and xylenes, this phenomenon should be further studied. In contrast to biogenic emissions dominating temperature-driven increases in OH reactivity and O_3 formation in Los Angeles[33], our findings emphasize that the temperature effects on evaporative AVOC emissions are equally important in Shanghai. Notably, biogenic emissions are suppressed at extremely high temperatures and are uncontrollable, highlighting the relatively significant impact of elevated AVOC emissions during heatwaves, which will amplify the O_3 climate penalty and pose a greater challenge to improving air quality and public health in megacities.

Online content

Any methods, additional references, Nature Portfolio reporting summaries, source data, extended data, supplementary information, acknowledgements, peer review information; details of author contributions and competing interests; and statements of data and code availability are available at https://doi.org/10.1038/s41561-024-01608-w.

References

1. Jerrett, M. et al. Long-term ozone exposure and mortality. *N. Engl. J. Med.* **360**, 1085–1095 (2009).
2. Feng, Z. et al. Ozone pollution threatens the production of major staple crops in East Asia. *Nat. Food* **3**, 47–56 (2022).
3. Seinfeld, J. H. & Pandis, S. N. *Atmospheric Chemistry and Physics: From Air Pollution to Climate Change* (John Wiley & Sons, 2016).
4. McDonald, B. C. et al. Volatile chemical products emerging as largest petrochemical source of urban organic emissions. *Science* **359**, 760–764 (2018).
5. Li, M. et al. Persistent growth of anthropogenic non-methane volatile organic compound (NMVOC) emissions in China during 1990–2017: drivers, speciation and ozone formation potential. *Atmos. Chem. Phys.* **19**, 8897–8913 (2019).
6. Wang, W. et al. Long-term trend of ozone pollution in China during 2014–2020: distinct seasonal and spatial characteristics and ozone sensitivity. *Atmos. Chem. Phys.* **22**, 8935–8949 (2022).
7. Koplitz, S. et al. Changes in ozone chemical sensitivity in the United States from 2007 to 2016. *ACS Environ. Au* **2**, 206–222 (2022).
8. Han, H. et al. Narrowing differences in urban and nonurban surface ozone in the Northern Hemisphere over 1990–2020. *Environ. Sci. Technol. Lett.* **10**, 410–417 (2023).
9. Watts, N. et al. The 2020 report of The Lancet Countdown on health and climate change: responding to converging crises. *Lancet* **397**, 129–170 (2021).
10. Ban, J., Lu, K., Wang, Q. & Li, T. Climate change will amplify the inequitable exposure to compound heatwave and ozone pollution. *One Earth* **5**, 677–686 (2022).
11. Hou, P. & Wu, S. Long-term changes in extreme air pollution meteorology and the implications for air quality. *Sci. Rep.* **6**, 23792 (2016).
12. Steiner, A. L. et al. Observed suppression of ozone formation at extremely high temperatures due to chemical and biophysical feedbacks. *Proc. Natl Acad. Sci. USA* **107**, 19685–19690 (2010).
13. Gu, Y., Li, K., Xu, J., Liao, H. & Zhou, G. Observed dependence of surface ozone on increasing temperature in Shanghai, China. *Atmos. Environ.* **221**, 117108 (2020).
14. Pfannerstill, E. Y. et al. Temperature-dependent emissions dominate aerosol and ozone formation in Los Angeles. *Science* **384**, 1324–1329 (2024).
15. Cao, C. et al. Policy-related gains in urban air quality may be offset by increased emissions in a warming climate. *Environ. Sci. Technol.* **57**, 9683–9692 (2023).
16. Nussbaumer, C. M. & Cohen, R. C. Impact of OA on the temperature dependence of $PM_{2.5}$ in the Los Angeles Basin. *Environ. Sci. Technol.* **55**, 3549–3558 (2021).
17. Pusede, S. et al. On the temperature dependence of organic reactivity, nitrogen oxides, ozone production, and the impact of emission controls in San Joaquin Valley, California. *Atmos. Chem. Phys.* **14**, 3373–3395 (2014).
18. Yamada, H., Inomata, S. & Tanimoto, H. Refueling emissions from cars in Japan: compositions, temperature dependence and effect of vapor liquefied collection system. *Atmos. Environ.* **120**, 455–462 (2015).
19. Rubin, J. I., Kean, A. J., Harley, R. A., Millet, D. B. & Goldstein, A. H. Temperature dependence of volatile organic compound evaporative emissions from motor vehicles. *J. Geophys. Res. Atmos.* **111**, D03305 (2006).
20. Huang, J. et al. Quantification of temperature dependence of vehicle evaporative volatile organic compound emissions from different fuel types in China. *Sci. Total Environ.* **813**, 152661 (2022).
21. Lin, C.-C., Yu, K.-P., Zhao, P. & Whei-May Lee, G. Evaluation of impact factors on VOC emissions and concentrations from wooden flooring based on chamber tests. *Build. Environ.* **44**, 525–533 (2009).
22. Liang, W., Yang, S. & Yang, X. Long-term formaldehyde emissions from medium-density fiberboard in a full-scale experimental room: emission characteristics and the effects of temperature and humidity. *Environ. Sci. Technol.* **49**, 10349–10356 (2015).
23. Xiong, J., Wei, W., Huang, S. & Zhang, Y. Association between the emission rate and temperature for chemical pollutants in building materials: general correlation and understanding. *Environ. Sci. Technol.* **47**, 8540–8547 (2013).
24. Huangfu, Y. et al. Diel variation of formaldehyde levels and other VOCs in homes driven by temperature dependent infiltration and emission rates. *Build. Environ.* **159**, 106153 (2019).

25. Meehl, G. A. & Tebaldi, C. More intense, more frequent, and longer lasting heat waves in the 21st century. *Science* **305**, 994–997 (2004).
26. Guo, H. et al. Tropospheric volatile organic compounds in China. *Sci. Total Environ.* **574**, 1021–1043 (2017).
27. Han, Y. et al. Measurement report: volatile organic compound characteristics of the different land-use types in Shanghai: spatiotemporal variation, source apportionment and impact on secondary formations of ozone and aerosol. *Atmos. Chem. Phys.* **23**, 2877–2900 (2023).
28. Peng, Y. et al. Observation-based sources evolution of non-methane hydrocarbons (NMHCs) in a megacity of China. *J. Environ. Sci.* **124**, 794–805 (2023).
29. Pu, X. et al. Enhanced surface ozone during the heat wave of 2013 in Yangtze River Delta region, China. *Sci. Total Environ.* **603-604**, 807–816 (2017).
30. Liu, Y. et al. Source profiles of volatile organic compounds (VOCs) measured in China: part I. *Atmos. Environ.* **42**, 6247–6260 (2008).
31. Yuan, B., Shao, M., Lu, S. & Wang, B. Source profiles of volatile organic compounds associated with solvent use in Beijing, China. *Atmos. Environ.* **44**, 1919–1926 (2010).
32. Niu, Z. et al. Temperature dependence of source profiles for volatile organic compounds from typical volatile emission sources. *Sci. Total Environ.* **751**, 141741 (2021).
33. Pfannerstill, E. Y. et al. Comparison between spatially resolved airborne flux measurements and emission inventories of volatile organic compounds in Los Angeles. *Environ. Sci. Technol.* **57**, 15533–15545 (2023).
34. Liu, Y. et al. Characteristics and sources of volatile organic compounds (VOCs) in Shanghai during summer: implications of regional transport. *Atmos. Environ.* **215**, 116902 (2019).
35. Gentner, D. et al. Emissions of organic carbon and methane from petroleum and dairy operations in California's San Joaquin Valley. *Atmos. Chem. Phys.* **14**, 4955–4978 (2014).
36. Khare, P. et al. Ammonium adduct chemical ionization to investigate anthropogenic oxygenated gas-phase organic compounds in urban air. *Atmos. Chem. Phys.* **22**, 14377–14399 (2022).
37. Coggon, M. M. et al. Volatile chemical product emissions enhance ozone and modulate urban chemistry. *Proc. Natl Acad. Sci. USA* **118**, e2026653118 (2021).
38. Seltzer, K. M. et al. Reactive organic carbon emissions from volatile chemical products. *Atmos. Chem. Phys.* **21**, 5079–5100 (2021).
39. Wang, S. et al. Emission characteristics of reactive organic gases (ROGs) from industrial volatile chemical products (VCPs) in the Pearl River Delta (PRD), China. *Atmos. Chem. Phys.* **24**, 7101–7121 (2024).
40. Li, K. et al. Ozone pollution in the North China Plain spreading into the late-winter haze season. *Proc. Natl Acad. Sci. USA* **118**, e2015797118 (2021).
41. Schnell, R. C. et al. Rapid photochemical production of ozone at high concentrations in a rural site during winter. *Nat. Geosci.* **2**, 120–122 (2009).
42. Qu, H. et al. Chemical production of oxygenated volatile organic compounds strongly enhances boundary-layer oxidation chemistry and ozone production. *Environ. Sci. Technol.* **55**, 13718–13727 (2021).
43. Tan, Z. et al. Daytime atmospheric oxidation capacity in four Chinese megacities during the photochemically polluted season: a case study based on box model simulation. *Atmos. Chem. Phys.* **19**, 3493–3513 (2019).
44. Wang, W. et al. Ozone pollution mitigation strategy informed by long-term trends of atmospheric oxidation capacity. *Nat. Geosci.* **17**, 20–25 (2024).
45. Lin, Y. C. et al. Summertime formaldehyde observations in New York City: ambient levels, sources and its contribution to HO_x radicals. *J. Geophys. Res. Atmos.* **117**, D08305 (2012).
46. Chang, X. et al. Full-volatility emission framework corrects missing and underestimated secondary organic aerosol sources. *One Earth* **5**, 403–412 (2022).
47. Khare, P. & Gentner, D. R. Considering the future of anthropogenic gas-phase organic compound emissions and the increasing influence of non-combustion sources on urban air quality. *Atmos. Chem. Phys.* **18**, 5391–5413 (2018).
48. Yan, L. et al. Evaporation process dominates vehicular NMVOC emissions in China with enlarged contribution from 1990 to 2016. *Environ. Res. Lett.* **16**, 124036 (2021).

[1]Jiangsu Key Laboratory of Atmospheric Environment Monitoring and Pollution Control, Collaborative Innovation Centre of Atmospheric Environment and Equipment Technology, Joint International Research Laboratory of Climate and Environment Change, Nanjing University of Information Science and Technology, Nanjing, China. [2]State Environmental Protection Key Laboratory of Formation and Prevention of Urban Air Pollution Complex, Shanghai Academy of Environmental Sciences, Shanghai, China. [3]Collaborative Innovation Center on Forecast and Evaluation of Meteorological Disasters, NUIST Center on Atmospheric Environment, Nanjing University of Information Science and Technology, Nanjing, China. [4]State Key Joint Laboratory of Environmental Simulation and Pollution Control, College of Environmental Sciences and Engineering, Peking University, Beijing, China. [5]Shanghai Key Laboratory of Atmospheric Particle Pollution and Prevention, Department of Environmental Science and Engineering, Fudan University, Shanghai, China. [6]School of Life and Environmental Science, Guilin University of Electronic Technology, Guilin, China. [7]School of Environment and Energy, South China University of Technology, Guangzhou, China. [8]School of Energy and Environment, Southeast University, Nanjing, China. [9]Office of Research and Development, US Environmental Protection Agency, Durham, NC, USA. [10]Shanghai Environmental Monitoring Centre, Shanghai, China. [11]John A. Paulson School of Engineering and Applied Sciences, Harvard University, Cambridge, MA, USA. ✉e-mail: jianlinhu@nuist.edu.cn

Methods

VOC and meteorological measurements

In this study, a dataset containing field measurements of 55 VOCs at the SAES (31.17° N, 121.43° E) site in Shanghai on an hourly basis during the summers (from June to August) of 2018–2020 was analysed. VOCs (including cyclopentane, 2-methylpentane and 3-methylhexane) with concentrations consistently below the detection limits were removed. The SAES site is in an urban environment with industrial sources ~50 km to the south and southwest (predominantly upwind) of the site. The VOCs, consisting of C_2–C_{12} hydrocarbons, were measured with an online gas chromatograph with a flame ionization detector, with measurement procedures and data quality assurance and quality control methods detailed elsewhere[28]. These VOCs were mapped to lumped VOC species in the chemical mechanism SAPRC07tic[49] to condense the findings and compare them with the model outputs (Supplementary Table 3). In addition, we used network measurements of NO_2 and O_3 concentrations at sites supervised by the China National Environmental Monitoring Centre (Sites 1141A–1150A in Shanghai and Sites 1223A–1233A and 3556A–3557A in Hangzhou).

All meteorological data for model evaluation (Supplementary Table 10) were obtained from the website (https://q-weather.info/), which collects measurements of meteorological factors (air temperature, wind speed and direction, humidity, precipitation and so on) from multiple sources that are available to the public. The measured hourly air temperature at a location (31.23° N, 121.53° E) near the SAES site was chosen to match the VOC measurements over time for the analysis of VOC–temperature relationships.

The dependence of measured VOCs on temperature

To remove the effects of dilution on VOC concentrations, the VOC ERs, as defined in ref. 50, were adopted. The ERs of VOCs relative to acetylene (ACYE) were calculated as follows:

$$\mathrm{ER_{VOC}} = \frac{\Delta[\mathrm{VOC}]}{\Delta[\mathrm{ACYE}]} = \frac{[\mathrm{VOC}] - [\mathrm{VOC_{bg}}]}{[\mathrm{ACYE}] - [\mathrm{ACYE_{bg}}]} \quad (1)$$

where Δ[VOC] is the excess concentration of an individual VOC over its background and [VOC] and [VOC_{bg}] denote the measured and background concentrations, respectively. The background concentration (ambient levels in the absence of local emission sources) is estimated as the minimum typical concentration in a location[51]. Here the background concentration of a VOC was determined from the tenth percentile of its hourly measurements over the study period; Δ[ACYE], [ACYE] and [$ACYE_{bg}$] in equation (1) were estimated analogously. In addition, only measurements on weekdays were examined to rule out the impacts of reduced emissions on weekends.

The ERs of individual VOCs and air temperatures in pairs were sorted into ten temperature bins to identify VOC–temperature relationships. Each bin contained the same number of samples (paired ERs and temperatures) and was represented by the average temperatures and ERs with outliers removed. High (low) outliers denote values over 1.5 times the interquartile range above (below) the third (first) quartile, which are likely to represent episodic events that do not reflect typical conditions and were thus removed from the analysis. The VOC concentrations were analysed analogously and showed similar patterns to those of the ERs with respect to the trends with temperature (Supplementary Fig. 2).

CMAQ model configurations

The CMAQ modelling system v.5.3 (ref. 52) was utilized to assess the impacts of temperature-driven emissions on ambient VOCs and O_3 during the summertime period from 25 May to 31 August 2018, including one week for initialization. The gas phase and aerosol chemistry were represented by the SAPRC07tic mechanism[53] and the AERO7 module, respectively. The simulations were conducted over three nested domains with grid spacings of 36 km, 12 km and 4 km, with the innermost domain encompassing the entire YRD, a highly industrialized and populated area in East China (Supplementary Fig. 18). The 2017 Multiresolution Emission Inventory for China (http://www.meicmodel.org) was employed to describe anthropogenic emissions in the 36 km and 12 km simulations, while the 4 km simulation utilized a high-resolution emissions inventory for the YRD[54]. Biogenic emissions were estimated using the Model for Emissions of Gases and Aerosols from Nature v.2.1 (ref. 55). In addition, the CMAQ model was driven by the Weather Research and Forecasting model v.4.1 for meteorological inputs.

The process analysis (PA) tool[56] in the CMAQ was employed to delve deeper into the evolution of air pollutants. Specifically, the integrated process rates output by the PA tool were utilized to identify the individual processes (for example, emissions, transport, chemistry, deposition) governing the accumulation and removal of VOCs in ambient air. In addition, the integrated reaction rates were applied to quantify (1) the primary sources of RO_x radicals ($RO_x = OH + HO_2 + RO_2$), stemming predominantly from the photolysis of HONO, O_3, HCHO and other carbonyl compounds, and alkene ozonolysis; and (2) the formation or loss rates of odd oxygen ($O_x = NO_2 + O_3$), where NO_2 was treated as an O_3 reservoir due to rapid conversion of NO to NO_2 by reacting with O_3 and subsequent release of O_3 via photolysis during the day. The formation of O_x ($F(O_x)$) summed up the reaction rates of all reactions in which O_3 or NO_2 acted as products in the SAPRC-07tic mechanism, while the loss of O_x ($L(O_x)$) encompassed reactions where O_3 and NO_2 acted as reactants. The net O_x change rates ($P(O_x)$) were determined as the difference between $F(O_x)$ and $L(O_x)$ (equation (2)), with positive (negative) values indicating net formation (destruction).

$$P(O_x) = F(O_x) - L(O_x) \quad (2)$$

In addition, the source-oriented CMAQ model[57] was employed to differentiate O_3 formed from local emissions in the YRD from that contributed by transported emissions from upwind sources or background. Since the focus of this study was on the impact of VOC emissions on O_3 formation, the high-order decoupled direct method[58] within the CMAQ model was used to estimate the contributions of individual VOC sources, utilizing sensitivity coefficients derived from high-order decoupled direct method and Taylor expansions. The VOC sources analysed include evaporative AVOC emissions (VCP-related sources and gasoline evaporation), other AVOC emissions (fossil fuel combustion, industrial activities and so on) and biogenic emissions. The first-order and second-order sensitivity coefficients provided insights into how O_3 responds to perturbations in VOC or NO_x emissions, and how these responses would change with reduced precursor emissions, respectively.

Emissions scenarios and impact attribution

In general, two model runs, with all inputs and model configurations identical except AVOC emissions over the innermost domain, were conducted in parallel, referred to as the base case and the adj case (Supplementary Table 11). The base case assumed constant, temperature-independent AVOC emissions as a function of the day of the week, as in a traditional manner. However, the adj case accounted for variations in AVOC emissions from day to day with daily maximum temperatures (see the toluene emissions as an example in Supplementary Fig. 19). As such, the differences between the two cases (including simulated concentrations and PA outputs) reflected the impacts of temperature-driven AVOC emissions.

In the base case, we attributed the relative enhancements during heatwaves compared with the monthly averages with meteorological factors (specifically, changes in pollutant or precursor dilution,

stronger solar radiation conducive to photochemistry and accelerated reaction rates at higher temperatures) or biogenic emissions changes. To further disentangle these impacts, we conducted a sensitivity test for the heatwave period. In this test simulation, the biogenic emissions input was replaced with monthly average biogenic emissions (referred to as the HW_biog case in Supplementary Table 11) compared with the base case, isolating the enhancements caused by meteorological factors alone.

The total enhancement (ENH_{tot}), meteorology-related enhancement (ENH_{met}) and biogenic emissions-induced enhancement (ENH_{biog}) of OH reactivity were estimated as follows:

$$ENH_{tot} = \left(\frac{VOCR_{HW}}{VOCR_{MM}} - 1\right)_{adj} \times 100\% \quad (3)$$

$$ENH_{met} = \left(\frac{VOCR_{HW\_biog}}{VOCR_{MM}} - 1\right)_{base} \times 100\% \quad (4)$$

$$ENH_{biog} = \left(\frac{VOCR_{HW}}{VOCR_{MM}} - 1\right)_{base} \times 100\% - ENH_{met} \quad (5)$$

where $VOCR_{HW}$ ($VOCR_{HW\_biog}$) represents the OH reactivity during the heatwave (with monthly average biogenic emissions) and $VOCR_{MM}$ denotes the monthly average. The enhancement driven by AVOC emissions ($ENH_{anthrop}$) was estimated as the difference between ENH_{tot} and the sum of ENH_{met} and ENH_{biog}:

$$ENH_{anthrop} = ENH_{tot} - ENH_{met} - ENH_{biog} \quad (6)$$

Similarly, the individual effects of variations in AVOC emissions, BVOC emissions and meteorological conditions on changes in daytime $P(RO_x)$, O_3 concentrations and $P(O_x)$ during heatwaves were estimated.

In addition to the aforementioned simulations with current emissions, five emissions scenarios were established (with or without temperature-induced adjustments) to predict O_3 changes and assess the impacts of temperature-driven AVOC emissions changes during heatwaves under various future emissions reduction policies. These scenarios include (1) a 50% reduction in total AVOC emissions, (2) a 50% reduction in evaporative AVOC emissions from non-combustion sources, (3) a 50% reduction in NO_x emissions, (4) a simultaneous reduction in both AVOC and NO_x emissions of 50% and (5) a 50% reduction in evaporative emissions of AVOCs and NO_x emissions.

Treatment of temperature-driven AVOC emissions in the model

Temperature-driven AVOC emissions are mainly from non-combustion sources, including solvent evaporation in the manufacturing and use of VCPs, gasoline evaporation from vehicles, and fuel evaporation during storage and transport. Our study is limited by a lack of experimental data on VOC emission rates as a function of temperature for all sources. Therefore, we focused specifically on VCP-related sources and gasoline evaporation due to (1) the availability of experimental data and (2) their significant contribution (>50%) to the region-wide emissions of aromatics that are strongly sensitive to temperature in the YRD (Supplementary Fig. 4). These sources were confirmed to be temperature-dependent in Shanghai, New York[15] and Los Angeles[16].

VCP-related emissions. We assumed that the magnitude of VOC emissions from VCPs, including industrial and residential solvent use, as categorized in ref. 54, would change with temperature according to equation (7). This equation was derived on the basis of measured emission rates of total VOCs from solvent-based paints at various temperatures in the laboratory and is identical in form to that used in ref. 20 (the study of which focused on vehicular emissions due to diurnal loss and was contributed by the same research group):

$$E_{sol} = \frac{1.3 \times 10^{12} \times e^{\frac{-4689}{T}}}{T} \quad (7)$$

where E_{sol} is the fitted emission rate from paints (in units of μg m^{-3} h^{-1}) and T is the ambient temperature (K).

In the experiment, the applied analytical system consisted of a headspace autosampler equipped with a gas chromatography–mass spectrometer (Shimadzu) utilizing an InertCap Pure-Wax column (30 m × 0.25 mm id × 0.25 μm film thickness). The column temperature was held at 35 °C for 8 minutes, and the temperature was subsequently increased to 250 °C at a rate of 15 °C min^{-1}. The mass spectrometer was operated within a mass range of 33–300 amu.

To characterize changes in VOC emissions with temperature, 10 ml samples of solvent-based paint were stored in sealed headspace vials and placed at specified temperatures (25 °C, 40 °C, 50 °C and 60 °C). The gas from paint evaporation within the headspace vials was sampled and injected into the gas chromatography–mass spectrometer instrument for the quantitative analysis of VOCs. The experiment revealed an increase in total VOC emissions by a factor of ~2 from solvent-based paint at 40 °C relative to that at 25 °C (Supplementary Fig. 20), equivalent to an increase of ~6.7% $°C^{-1}$. This increase is comparable to the variation in vehicular emissions with temperature (increase of 6.5% $°C^{-1}$) in ref. 19.

Gasoline evaporation. Evaporative emissions from vehicles (specifically, emissions from refuelling loss, running loss, hot soak and diurnal loss) were dominated by running loss[59]. Here variations in vehicular non-tailpipe emissions were considered on the basis of the fitting of running losses from light-duty vehicles with a fuel volatility of 8.0 psi in Reid vapour pressure at different temperatures in MOBILE6 (ref. 60) (Supplementary Fig. 21). The emission factors (E_{gas} in equation (8), in units of g mi^{-1}) were depicted as a function of temperature (T in equation (8), in units of °C), corresponding to an increase of ~3.1% $°C^{-1}$ in the temperature range of 25–40 °C.

$$E_{gas} = 0.003T^2 - 0.10T + 3.6 \quad (8)$$

Emissions adjustments. The evaporative VOC emissions at a specific temperature were estimated by adjusting the emissions inventory under the assumption that the emissions inventory represents emissions at 25 °C. The scaling factors $F(T)$ were determined using equation (9).

$$F(T) = \frac{E(T)}{E(T_{ref})} \quad (9)$$

where T_{ref} = 25 °C and $E(T)$ and $E(T_{ref})$ were estimated using equations (7) and (8) for VCP-related emissions and gasoline evaporation, respectively. The daily VOC emissions were adjusted on the basis of the daily maximum temperature. Importantly, the VOC emissions from industrial solvent use were estimated using the mass-balanced method[54], indicating that the annual emissions should be mass conserved. As a result, the seasonal cycle of emissions could be altered. Other VOC emissions were considered temperature-independent and remained unchanged in the simulations.

Data availability

All data that support the findings of this study are included in this published paper (and its Supplementary Information) and are available via Figshare at https://doi.org/10.6084/m9.figshare.26106289.

Code availability

The source code of the CMAQ model used in this study is publicly available at https://github.com/USEPA/CMAQ. Additional codes, including Fortran code and R scripts for processing the observational data, emissions and CMAQ outputs, are available from the corresponding author on request.

References

49. Carter, W. P. Development of the SAPRC-07 chemical mechanism. *Atmos. Environ.* **44**, 5324–5335 (2010).
50. Warneke, C. et al. Multiyear trends in volatile organic compounds in Los Angeles, California: five decades of decreasing emissions. *J. Geophys. Res. Atmos.* **117**, D00V7 (2012).
51. McCarthy, M. C., Hafner, H. R. & Montzka, S. A. Background concentrations of 18 air toxics for North America. *J. Air Waste Manage. Assoc.* **56**, 3–11 (2006).
52. Appel, K. W. et al. The Community Multiscale Air Quality (CMAQ) model versions 5.3 and 5.3.1: system updates and evaluation. *Geosci. Model Dev.* **14**, 2867–2897 (2021).
53. Xie, Y. et al. Understanding the impact of recent advances in isoprene photooxidation on simulations of regional air quality. *Atmos. Chem. Phys.* **13**, 8439–8455 (2013).
54. An, J. et al. Emission inventory of air pollutants and chemical speciation for specific anthropogenic sources based on local measurements in the Yangtze River Delta region, China. *Atmos. Chem. Phys.* **21**, 2003–2025 (2021).
55. Guenther, A. B. et al. The Model of Emissions of Gases and Aerosols from Nature version 2.1 (MEGAN2. 1): an extended and updated framework for modeling biogenic emissions. *Geosci. Model Dev.* **5**, 1471–1492 (2012).
56. Gipson, G. Process analysis. In *Science Algorithms of the EPA Models—3 Community Multiscale Air Quality (CMAQ) Modeling System* (eds Byun, D. W. & Ching, J. K. S.) Ch. 16 (United States Environmental Protection Agency, 1999).
57. Li, L. et al. Modelling air quality during the EXPLORE-YRD campaign—part II. Regional source apportionment of ozone and $PM_{2.5}$. *Atmos. Environ.* **247**, 118063 (2021).
58. Cohan, D. S., Hakami, A., Hu, Y. & Russell, A. G. Nonlinear response of ozone to emissions: source apportionment and sensitivity analysis. *Environ. Sci. Technol.* **39**, 6739–6748 (2005).
59. Liu, H. et al. An updated emission inventory of vehicular VOCs and IVOCs in China. *Atmos. Chem. Phys.* **17**, 12709–12724 (2017).
60. *Evaporative Emissions from On-Road Vehicles in MOVES2014* (EPA, 2014).

Acknowledgements

This research was supported by the National Natural Science Foundation of China (42021004, 42107117, M.Q., Y.S. and J. Hu.; 42377095, Z.Y.). We acknowledge the Chinese Ministry of Science and Technology for their support through the Key Research and Development Program (2022YFC3701000, M.Q., S.G., M.H. and J. Hu; 2022YFE0136200, H.W. and J. Li; 2023YFC3706204, M.W.). Z.Y. acknowledges support by the Key-Area Research and Development Program of Guangdong Province (2020B1111360003). The views expressed in this article are those of the authors and do not necessarily reflect the views or policies of the US EPA.

Author contributions

J. Hu and M.Q. conceived and designed the work; M.Q. and Y.S. ran the simulations; M.Q., Y.S., M.W. and H.W. analysed and interpreted the data; H.W., J.A., J. Lu, Q.W., C.H., J. Huang and Z.Y. contributed materials/analysis tools; M.Q. and J. Hu led the writing; Y.C., Z.T., C.L., Z.L., X.X., J. Li, H.L., H.O.T.P., S.G., M.H., Y.Z. and D.J.J. contributed significantly to results discussion and paper editing.

Competing interests

The authors declare no competing interests.

Additional information

Extended data is available for this paper at https://doi.org/10.1038/s41561-024-01608-w.

Supplementary information The online version contains supplementary material available at https://doi.org/10.1038/s41561-024-01608-w.

Correspondence and requests for materials should be addressed to Jianlin Hu.

Peer review information *Nature Geoscience* thanks Peeyush Khare and the other, anonymous, reviewer(s) for their contribution to the peer review of this work. Primary Handling Editor: Xujia Jiang, in collaboration with the *Nature Geoscience* team.

https://doi.org/10.1038/s41561-024-01608-w

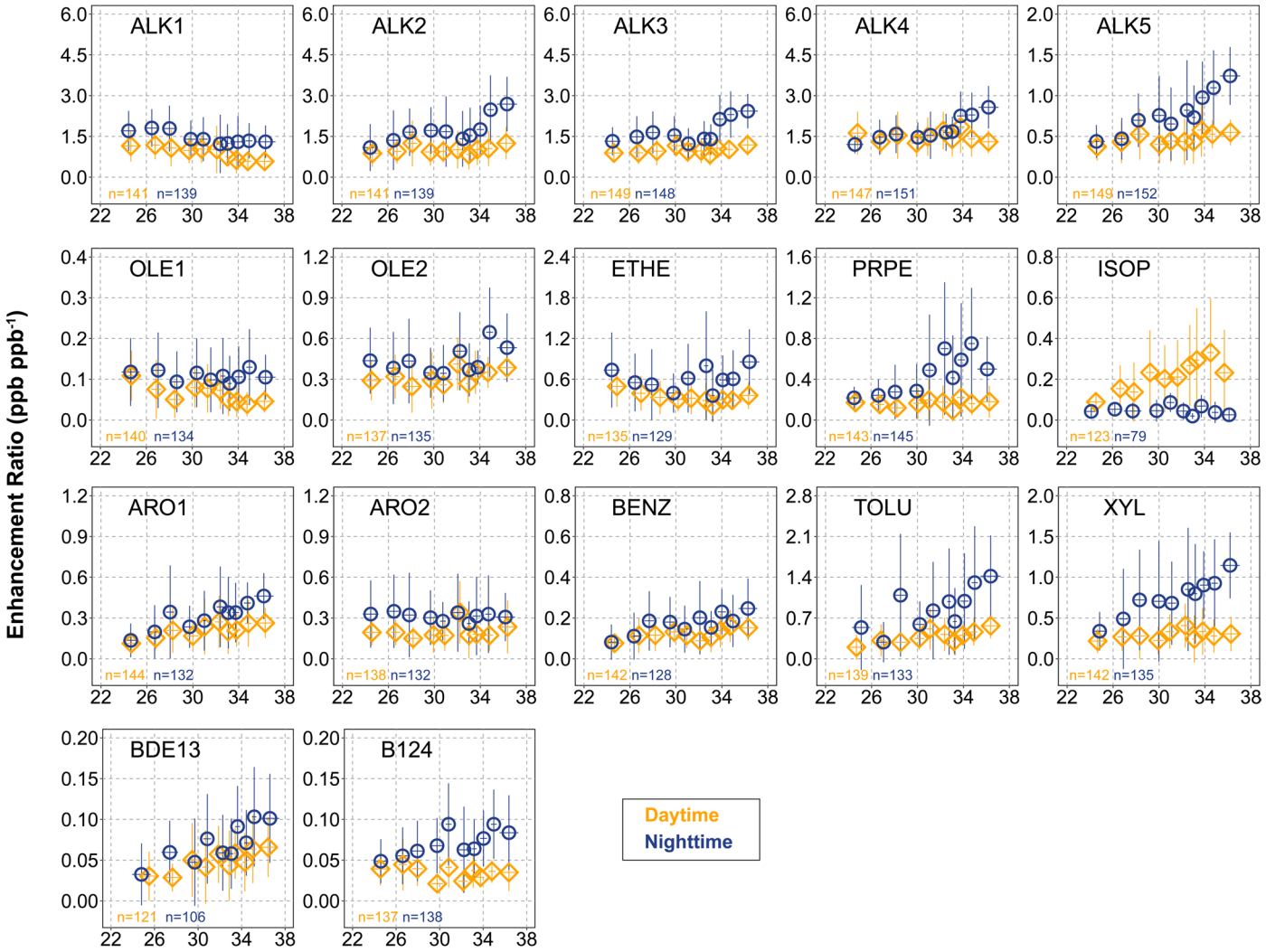

Extended Data Fig. 1 | Observed ERs of individual VOCs versus temperature during the summers of 2018–2020 in Shanghai. Daily ERs (with the sample size shown in the lower left corner of each panel) were split evenly into ten bins according to the paired temperatures. The average values for daytime and nighttime ERs in each bin are represented by yellow and blue open circles, respectively, with standard deviations (±1σ) represented by whiskers. The definitions of individual VOCs using the SAPRC07tic chemical mechanism are shown in Supplementary Table S3.

https://doi.org/10.1038/s41561-024-01608-w

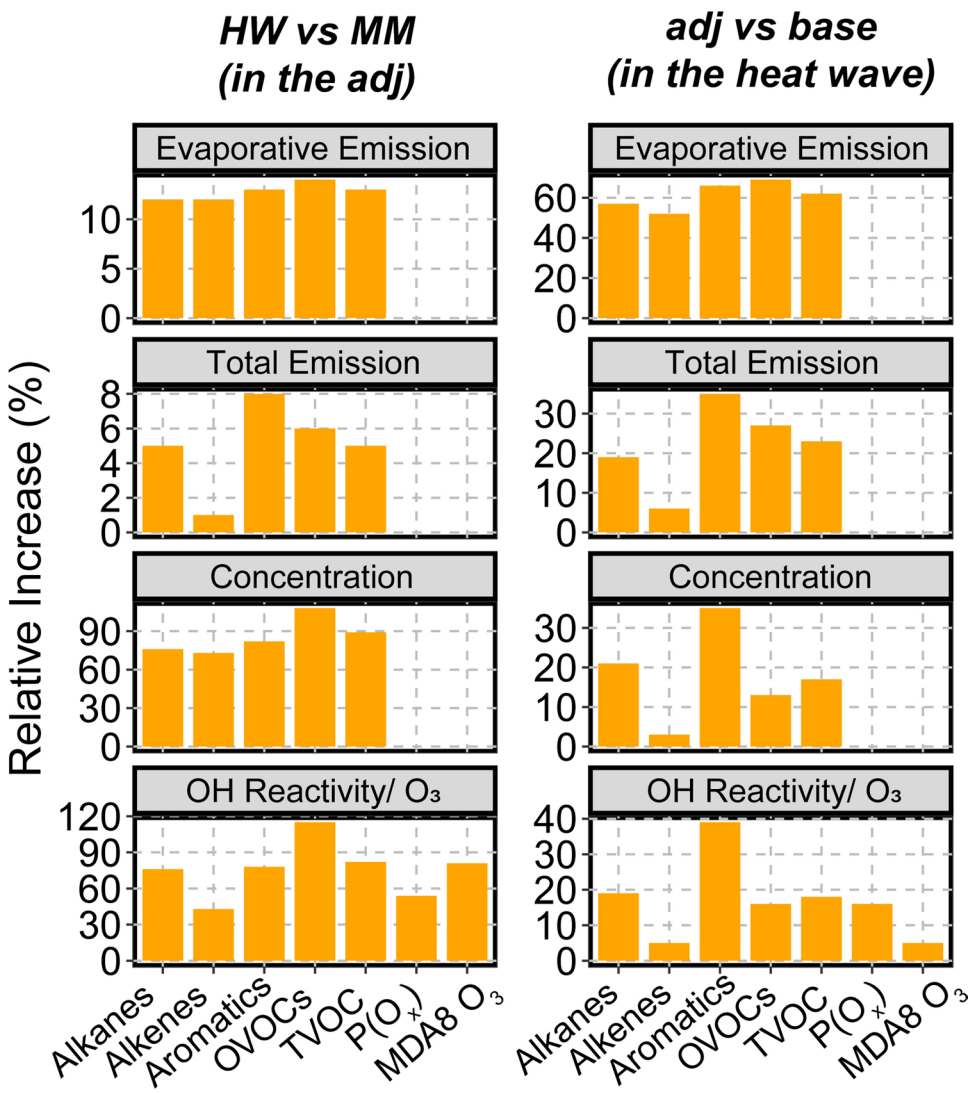

Extended Data Fig. 2 | Simulated increases in VOC emissions and concentrations, OH reactivity, O3 concentrations and net formation of Ox (P(Ox)) in Shanghai. The left column compares these variables during the heat wave (HW) relative to the monthly means (MM) in the adj case, while the right column compares the adj case to the base case during the heat wave.

https://doi.org/10.1038/s41561-024-01608-w

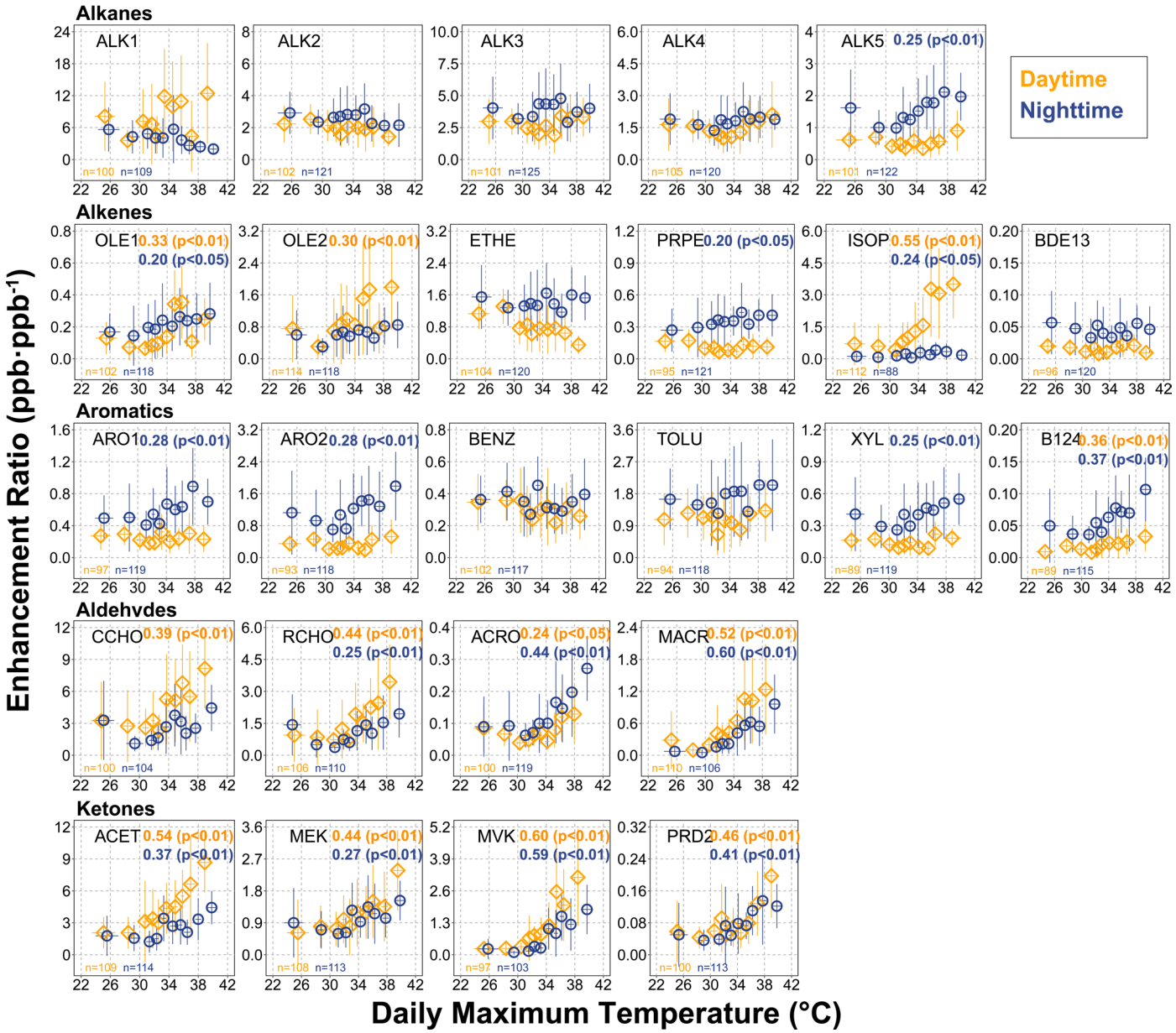

Extended Data Fig. 3 | Observed ERs of individual VOCs versus temperature during the summers of 2021–2023 in Hangzhou. The measurements were conducted at Zhejiang Ecological and Environmental Monitoring Centre. Only weekday data were included in the analysis. Similar to Extended Data Fig. 1, the sample sizes of daily ERs are shown in the lower left corner of each panel; bin-averaged ERs are represented by open circles, with standard deviations (±1σ) represented by whiskers. The yellow (daytime) and blue (nighttime) numbers in the upper right corner indicate the correlation coefficients of ERs with daily maximum temperatures, based on two-sided Pearson correlation tests. Only positive correlation coefficients that indicate statistically significant ($p < 0.05$) are shown for conciseness.

https://doi.org/10.1038/s41561-024-01608-w

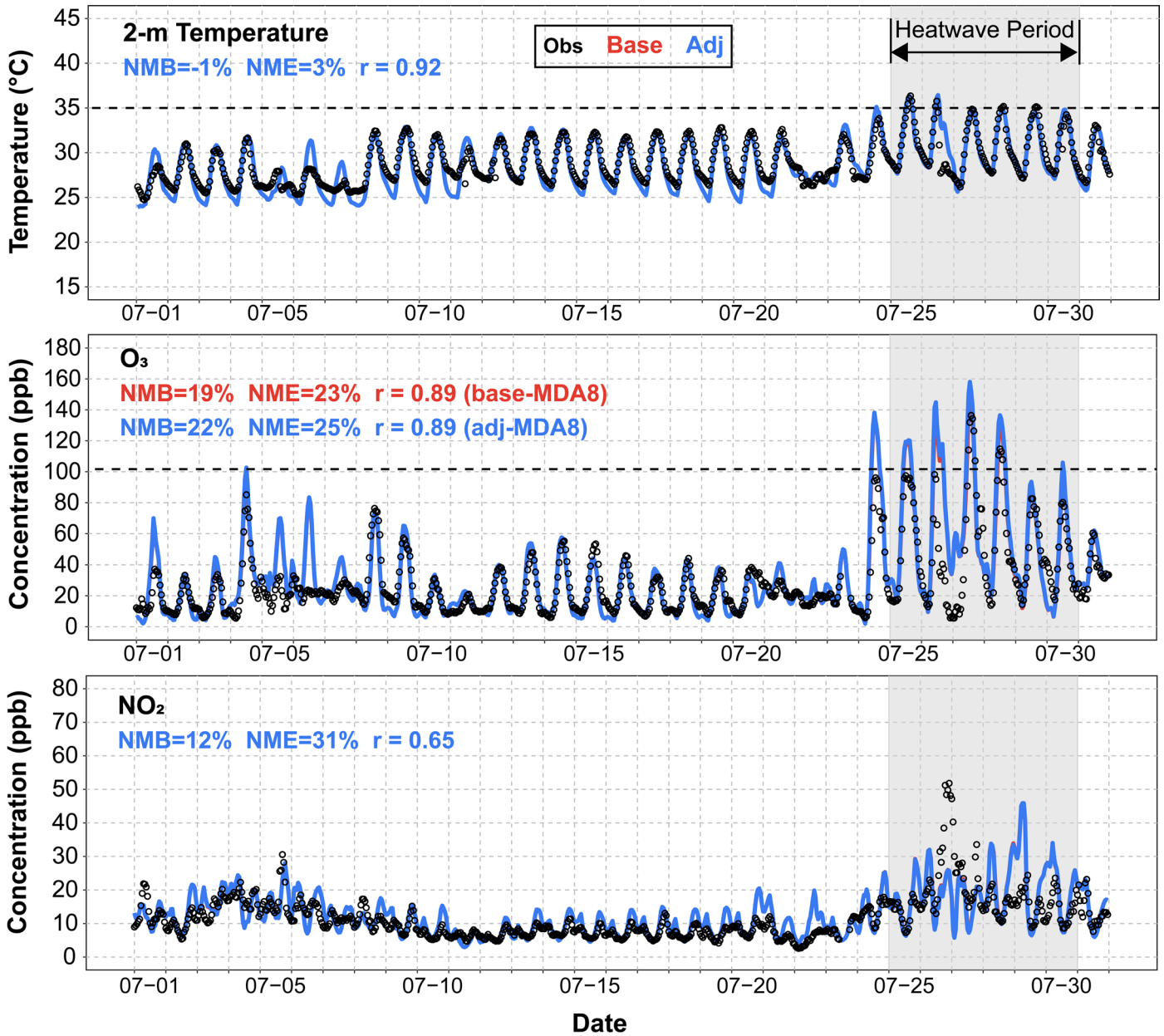

Extended Data Fig. 4 | Time series of measured and simulated temperature, O3 and NO2 for July 2018 in Shanghai. The data represent averages across all meteorological or the CNEMC sites in Shanghai. The heat wave, defined as at least three consecutive days with daily maximum temperatures exceeding 35 °C (indicated with a horizontal dashed line in the upper panel), occurred from July 25 to 30. The 1-hour O3 standard of 200 g·m − 3 (~ 101.7 ppb at 25 °C) is marked by a dashed line in the middle panel. The CMAQ model overestimated O3 exceedances on July 25–26, likely due to the high biases of air temperature on the two days preceding the heat wave and failure to capture precipitation on July 26. As a result, the simulations over July 25–26 were excluded in Fig. 3.

https://doi.org/10.1038/s41561-024-01608-w

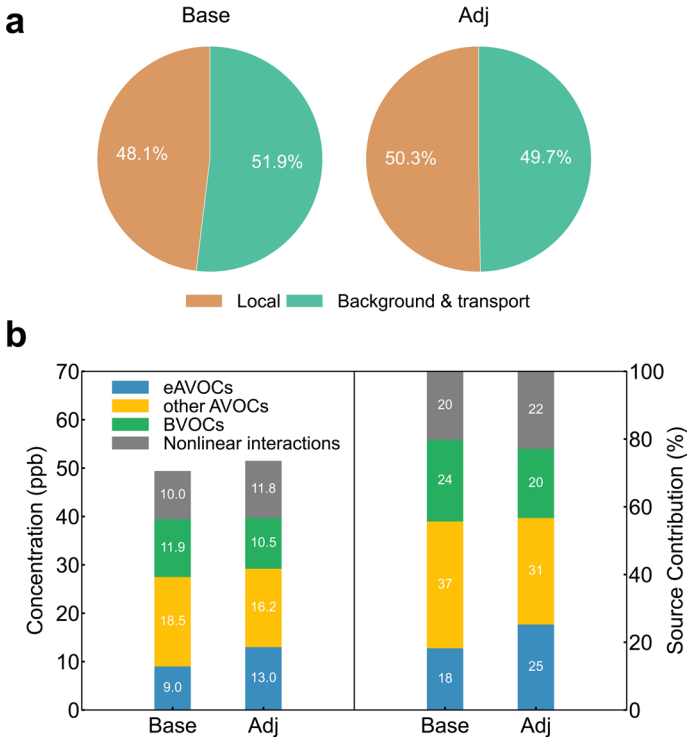

Extended Data Fig. 5 | Impact of local emissions on daytime O3 during the heat wave in Shanghai. a, Contribution of O3 from local emissions (within the YRD) compared to background/transported emissions from upwind sources. **b**, Contribution of region-wide VOC emissions to daytime O3, decomposed by individual sources.